Smart Structures and Systems, *Vol. 15, No. 4 (2015) 1063-1083*
DOI: http://dx.doi.org/10.12989/sss.2015.15.4.1063

The study on piezoelectric transducers: theoretical analysis and experimental verification

Chia-Chung Sung and Szu-Chi Tien*

Department of Mechanical Engineering, National Cheng-Kung University, 1 University Road, Tainan 701, Taiwan

(Received April 3, 2013, Revised January 26, 2014, Accepted March 30, 2014)

Abstract. The main purpose of this research is to utilize simple mathematical models to depict the vibration behavior and the resulted sound field of a piezoelectric disk for ultrasonic transducers. Instead of using 1-D vibration model, coupled effect between the thickness and the radial motions was considered to be close to the real vibration behavior. Moreover, Huygens-Fresnel principle was used in both incident and reflected waves to analyze the sound field under obstacles in finite distance. Results of the tested piezoelectric disk show that, discrepancies between the simulation and experiment are 2.5% for resonant frequency and 12% for resulted sound field. Therefore, the proposed method can be used to reduce the complexity in modeling vibration problems, and increase the reliability on analyzing piezoeletric transducers in the design stage.

Keywords: piezoelectric disk; ultrasonic transducer; vibration model; Huygens-Fresnel principle

1. Introduction

Piezoelectric material has the property for converting the electrical-energy to mechanical-energy and vice versa; therefore, it has been utilized often for building transducers. In particular, ultrasonic transducers made of piezoelectric materials have been applied on various fields such as sound field analysis (Wang 1996, Ding *et al.* 2003, Dugnani 2009, Gutierrez *et al.* 2012), structural damage detection/reduction (Lee *et al.* 2013, Zenz *et al.* 2013), position control (Kung 2002, Liu *et al.* 2012), and wave generation (Nowotny and Benes 1987, Lin *et al.* 2013, Martins *et al.* 2012). Since all applications listed above are related to the vibration behavior and the resulted sound field of piezoelectric transducers, a good understanding of their vibration behavior may help to improve their performance. Therefore, the main purpose of this research is to establish and verify mathematical models for properly depicting the vibration of piezoelectric transducers.

Vibration models of piezoelectric transducers have been studied a lot by researchers in the past couple decades. For example, the resonant frequency of a transducer could be expressed in an analytic form that was related to material properties (Tiersten 1963). Moreover, the steady state

*Corresponding author, Professor, E-mail: sctien@mail.ncku.edu.tw

http://www.techno-press.org/?journal=sss&subpage=8 ISSN: 1738-1584 (Print), 1738-1991 (Online)

vibration models with simple shapes such as flat plates and flat disks were well developed (Tiersten 1963, IEEE Standard 1987). On the other hand, finite element approaches were also utilized to analyze the dynamic behavior of piezoelectric transducers (Kunkel *et al.* 1990, Kocbach 2000, Guo *et al.* 1992).

However, when the dimensions in thickness and radial directions of a piezoelectric disk are in similar order, simple 1-D model is not enough to describe the vibration behavior precisely. In contrast, comprehensive understanding of coupled vibration analyses in the thickness and radial directions help to figure out the dynamic behavior. Lin in 1998 (Lin 1998) proposed a mechanical coupling coefficient, i.e., a ratio of stress between the thickness direction (z-axis) and its perpendicular direction (r-axis, θ-axis) as shown in Fig. 1, to derive the equivalent-coupled-vibration in two perpendicular directions. Although, this equivalence-based approach seemingly decoupled and simplified the original coupled vibration problem, it created another variable (i.e., the mechanical coupling coefficient) which required further experimental verification. Differently, Chi-Hung Huang *et al.* in 2004 (Huang *et al.* 2004) analytically derived the disk displacement in the thickness direction (z-axis) as a function of r-axis and θ-axis only based on plane stress assumption and showed consistency to the result of finite element analysis. Rather than requiring a mechanical coupling coefficient or a plane stress assumption in the thickness direction, Iula *et al.* in 1998 (Iula *et al.* 1998) described cylinder-shaped piezoceramic elements with an approximated coupled vibration model. The key point in their model is that coupled vibrations between the thickness and the radial directions were computed by complying the continuity-equation of integrated-stresses with the external forces. Although it is an approximated model, the predicted vibration behavior showed good consistency to experimental results.

Beside vibration behaviors of a piezoelectric disk, the induced sound field (which causes pressure then) in the thickness direction is also important in practical applications. Griffice and Seydel in 1981 (Griffice and Seydel 1981), with geometrical approximations, applied the concept of spherical-continuous-wave on a transducer to calculate the longitudinal and transverse ultrasonic fields. Cheeke in 2002 (Cheeke 2002) computed the steady-state sound field resulted from a uniformly-vibrating piston in an infinite space by Huygens-Fresnel principle. Cheeke stated that infinite sound point sources were envisioned to spread on the piston surface and each point source emitted spherical wave. Therefore, pressure at any position in the front can be viewed as the contributions from each sound point source.

In order to depict the vibration behavior and the resulted sound field of a piezoelectric disk well, merits proposed in early researches were integrated in this work. First of all, the approximate coupled vibration model of cylinder-shaped piezoceramic elements from Ref. (Iula *et al.* 1998) was adopted and integrated with the energy dissipation concept proposed by Lee *et al.* in 2004 (Lee *et al.*, 2004). In this part, a new problem-solving procedure is proposed and demonstrated to predict the vibration behavior at steady state. Secondly, the mathematical expression of the sound point source in Ref. (Cheeke 2002) was used to perform the Huygens-Fresnel principle for describing the sound propagation. In particular, the behavior of reflected pressure wave between the piezoelectric disk and the pressure sensor at steady state was studied for applications where an obstacle was placed in finite distance. Results of the tested piezoelectric disk show that, discrepancies between the simulation and experiment are 2.5% for resonant frequency and 12% for resulted sound field. Therefore, the novelty of this research is to propose a method that can be used to reduce the complexity in modeling vibration problems, and increase the reliability on analyzing piezoeletric transducers in the design stage.

The rest of the article is organized as follows. The theoretical analyses including piezoelectric disk vibration and sound propagation under obstacle are formulated in Section 2. Experimental results are presented with discussions in Section 3 and our conclusions are in Section 4.

2. Theoretical analyses

2.1 Coupled vibration model

For a piezoelectric transducer, vibration modes in different axes are coupled especially when its dimension in different axes are comparable. In particular, for a transversely isotropic piezoelectric disk, the coupled vibration between the thickness and radial axes are explored in this article based on Ref. (Iula *et al.* 1998).

Fig. 1 showed a piezoelectric disk with radius a and thickness b in cylindrical coordinate. The piezoelectric disk was coated with electrodes on the flat surfaces where an AC voltage $Ve^{j\omega t}$ was applied. In order to model the vibration behavior, three assumptions were made as follows. First, because of the electrode position, the induced electric field E_r and E_θ were assumed zero everywhere inside the piezoelectric disk. Second, due to geometric symmetry, all quantities are θ independent and the displacement u_θ is zero; therefore, the coordinate axes r and z are the directions where the pure-mode-vibration propagates, i.e., $u_r = u_r(r)$ and $u_z = u_z(z)$. Third, the electrical field is applied in the z –axis which results in the dominant deformation of the piezoelectric disk; therefore, energy dissipation is considered in z –axis only and described in terms of a viscosity coefficient η.

With assumptions shown above, the constitutive equations are simplified from Ref. (Ikeda 1990, Lee *et al.* 2004) and reduced to

$$T_{rr} = c_{11}^D S_{rr} + c_{12}^D S_{\theta\theta} + c_{13}^D S_{zz} - h_{31} D_z, \tag{1}$$

$$T_{\theta\theta} = c_{12}^D S_{rr} + c_{11}^D S_{\theta\theta} + c_{13}^D S_{zz} - h_{31} D_z, \tag{2}$$

$$T_{zz} = c_{13}^D S_{rr} + c_{13}^D S_{\theta\theta} + c_{33}^D S_{zz} + \eta \dot{S}_{zz} - h_{33} D_z, \tag{3}$$

$$E_z = -h_{31} S_{rr} - h_{31} S_{\theta\theta} - h_{33} S_{zz} + \beta_{33}^S D_z. \tag{4}$$

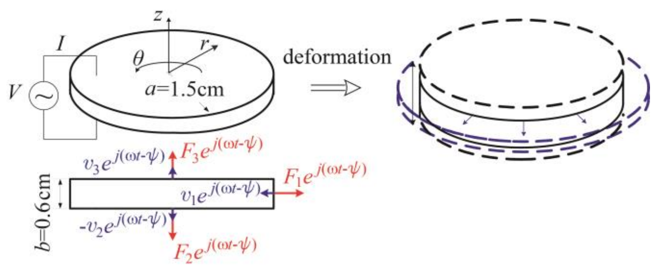

Fig. 1 Schematic diagram of a piezoelectric disk with an applied AC voltage. Where v_i is the surface vibration velocity, F_i is the surface force (i = 1, 2, 3)

Besides, the relations between the strain tensor and the displacement vector are

$$S_{rr} = \frac{\partial u_r}{\partial r}, \qquad S_{\theta\theta} = \frac{u_r}{r}, \qquad S_{zz} = \frac{\partial u_z}{\partial z}. \tag{5}$$

By Newton's 2nd law, motions in the radial and the thickness direction can be represented as

$$\frac{\partial T_{rr}}{\partial r} + \frac{T_{rr} - T_{\theta\theta}}{r} = \rho_{pzt} \frac{\partial^2 u_r}{\partial t^2}, \tag{6}$$

$$\frac{\partial T_{zz}}{\partial z} = \rho_{pzt} \frac{\partial^2 u_z}{\partial t^2}. \tag{7}$$

Substituting Eqs. (1),(2),(3) and (5) into Eqs. (6) and (7), the governing equations are

$$c_{11}^D \left[\frac{\partial^2 u_r}{\partial r^2} + \frac{1}{r}\frac{\partial u_r}{\partial r} - \frac{u_r}{r^2} \right] = \rho_{pzt} \frac{\partial^2 u_r}{\partial t^2}, \tag{8}$$

$$c_{33}^D \frac{\partial^2 u_z}{\partial z^2} + \eta \frac{\partial}{\partial t}\left(\frac{\partial^2 u_z}{\partial z^2} \right) = \rho_{pzt} \frac{\partial^2 u_z}{\partial t^2}. \tag{9}$$

To solve the entire vibration problem, a strategy to sequentially deal with the dissipative portion and reversible portion of the governing equations is used and elaborated as follows. At first, by utilizing the method of variables separation to set $u_z=H(z)G(t)$, Eq. (9) can be rewritten as

$$\frac{H''(z)}{H(z)} = \frac{\rho_{pzt}\ddot{G}(t)}{c_{33}^D G(t) + \eta \dot{G}(t)} = -K^2, \tag{10}$$

where K is a positive constant. In particular, the time related part of Eq. (10) forms a damped vibration equation

$$\ddot{G}(t) + 2\zeta\omega_n \dot{G}(t) + \omega_n^2 G(t) = 0, \tag{11}$$

where $\omega_n = \sqrt{\frac{c_{33}^D K^2}{\rho_{pzt}}}$ is the natural frequency and $\zeta = \frac{\eta K^2}{2\rho\omega_n}$ is the damping ratio.

Remark 1 In order to convert the piezoelectric disk to an equivalent mass-damper-spring system shown in Eq. (11), the constant K should be the reciprocal of the disk thickness, i.e., 153.85(1/m) in this research.

Now, when a harmonic voltage input $Ve^{j\omega t}$ is applied on the piezoelectric disk (i.e., a force term will be added in Eq. (11), the steady state solution can be expressed as

$$G(t) = XMe^{j(\omega t - \psi)} \tag{12}$$

where X is a constant to be determined, $M = \dfrac{1}{\left\{\left[1-(\omega/\omega_n)^2\right]^2 + \left[2\zeta\omega/\omega_n\right]^2\right\}^{1/2}}$ is the magnification factor, and $\psi = \tan^{-1}\left[\dfrac{2\zeta\omega/\omega_n}{1-(\omega/\omega_n)^2}\right]$ is the phase delay. Up to this point, the dissipative portion has been included in Eq. (12); therefore, only the reversible portion should be considered hereafter and Eqs. (3) and (9) can be simplified to be the following two equations, i.e.

$$T_{zz} = c_{13}^D S_{rr} + c_{13}^D S_{\theta\theta} + c_{33}^D S_{zz} - h_{33} D_z, \tag{13}$$

$$c_{33}^D \frac{\partial^2 u_z}{\partial z^2} = \rho_{pzt} \frac{\partial^2 u_z}{\partial t^2}. \tag{14}$$

Second, the steady state solutions of Eqs. (8) and (14) can be expressed as

$$u_r(r) = C_1 J_1(k_1 r) e^{j(\omega t-\psi)} + C_2 Y_1(k_1 r) e^{j(\omega t-\psi)} \tag{15}$$

$$u_z(z) = \left[C_3 \sin(k_3 z) + C_4 \cos(k_3 z)\right] e^{j(\omega t-\psi)} \tag{16}$$

where J_1 and Y_1 are the Bessel's function of the first kind of order one and second kind of order one, respectively. $k_1 = \dfrac{\omega}{c_1}$, $c_1 = \sqrt{\dfrac{c_{11}^D}{\rho_{pzt}}}$, $k_3 = \dfrac{\omega}{c_3}$, $c_3 = \sqrt{\dfrac{c_{33}^D}{\rho_{pzt}}}$ are in turn the wave number and the wave propagation velocity in the r and z directions.

The constants C_1, C_2, C_3 and C_4 can be determined with boundary conditions. According to Fig. 1, at the center of disk ($r = 0$), peripheral surface ($r = a$) and two flat surfaces ($z = 0$; $z = b$), one has

$$u_r(0) = finite, \quad \dot{u}_r(a) = v_1 e^{j(\omega t-\psi)}, \quad \dot{u}_z(0) = -v_2 e^{j(\omega t-\psi)}, \quad \dot{u}_z(b) = v_3 e^{j(\omega t-\psi)}$$

Then Eqs. (15) and (16) become

$$u_r(r) = \frac{v_1}{j\omega J_1(k_1 a)} J_1(k_1 r) e^{j(\omega t-\psi)} \tag{17}$$

$$u_z(z) = \frac{1}{j\omega}\left[\frac{v_3 + v_2\cos(k_3 b)}{\sin(k_3 b)}\sin(k_3 z) - v_2\cos(k_3 z)\right] e^{j(\omega t-\psi)} \tag{18}$$

Since forces should satisfy the continuity equation on boundaries, the force on every external surface of the disk is balanced by the integral of stresses, i.e.

$$\begin{aligned} \int_{A_1} T_{rr}(a)dA_1 &= F_1 e^{j(\omega t-\psi)} \\ \int_{A_2} T_{zz}(0)dA_2 &= F_2 e^{j(\omega t-\psi)} \\ \int_{A3} T_{zz}(b)dA_3 &= F_3 e^{j(\omega t-\psi)} \end{aligned} \tag{19}$$

where A_1, A_2, and A_3 are the areas of peripheral surface ($r = a$) and flat surfaces ($z = 0; z = b$).

Moreover, the electric displacement toward z-direction, D_z, is a function of time only and is a constant with respect to the z-coordinate (Tiersten 1963); therefore, the current i is

$$i = M\ Ie^{j(\omega t-\psi)} = A_2 \frac{\partial D_z}{\partial t}$$

and

$$D_z = \frac{M\ I}{j\omega\pi a^2} e^{j(\omega t-\psi)} \tag{20}$$

where MI is the amplitude of the current. Then, combination of Eqs. (1),(2),(5),(17),(18),(19), and (20) leads to

$$\begin{aligned} F_1 &= \frac{z_1(2\pi ab)}{j}\left[\frac{k_1 a J_0(k_1 a) - J_1(k_1 a)}{k_1 a J_1(k_1 a)} + \frac{c_{12}^D}{c_{11}^D k_1 a}\right] v_1 \\ &\quad + c_{13}^D \frac{2\pi a}{j\omega}(v_3 + v_2) - h_{31}\frac{2bMI}{j\omega a}, \\ F_2 &= \frac{2\pi a c_{13}^D v_1}{j\omega} + \frac{z_3(\pi a^2)}{j}\left[\frac{v_3}{\sin(k_3 b)} + \frac{v_2}{\tan(k_3 b)}\right] \\ &\quad - h_{33}\frac{MI}{j\omega}, \\ F_3 &= \frac{2\pi a c_{13}^D v_1}{j\omega} + \frac{z_3(\pi a^2)}{j}\left[\frac{v_3}{\tan(k_3 b)} + \frac{v_2}{\sin(k_3 b)}\right] \\ &\quad - h_{33}\frac{MI}{j\omega}, \end{aligned} \tag{21}$$

where $\frac{c_{11}^D k_1}{\omega} = \rho_{pzt} c_1 \equiv z_1$, $\frac{c_{33}^D k_3}{\omega} = \rho_{pzt} c_3 \equiv z_3$ are the specific acoustic impedances in r- and z-direction, respectively.

In order to relate the applied voltage $Ve^{j\omega t}$ to the vibration behavior of the piezoelectric disk, the electric field E_z in the z-direction should be solved first. By substituting Eqs. (17), (18), and (5) into (4), one has

$$\begin{aligned} E_z &= \frac{-h_{31}k_1}{j\omega}\frac{J_0(k_1 r)}{J_1(k_1 a)}v_1 e^{j(\omega t-\psi)} \\ &\quad -h_{33}\frac{1}{j\omega}\left[\frac{k_3(v_3+v_2\cos(k_3 b))}{\sin(k_3 b)}\cos(k_3 z)+k_3 v_2\sin(k_3 z)\right]e^{j(\omega t-\psi)} \\ &\quad +\beta_{33}^S\frac{MI}{j\omega\pi a^2}e^{j(\omega t-\psi)}. \end{aligned} \tag{22}$$

It can be seen that the electric field E_z obtained above is a function of r and z; therefore, in order to get an equivalent voltage for equi-potential, the voltage is computed by integrating the electrical field along r- and z-axis, and then taking average with the flat surface area (πa^2), i.e.

$$\begin{aligned} MVe^{j(\omega t-\psi)} &= \frac{1}{\pi a^2}\int_0^a\left[\int_0^b (Eqn.(22))dz\right]2\pi r dr \\ &= \frac{-2bh_{31}}{j\omega a}v_1 e^{j(\omega t-\psi)} - h_{33}\frac{(v_3+v_2)}{j\omega}e^{j(\omega t-\psi)} + \frac{MI}{j\omega C_0}e^{j(\omega t-\psi)} \end{aligned} \tag{23}$$

where $C_0 = \dfrac{\pi a^2}{\beta_{33}^S b}$.

In summary, the mechanical and electrical characteristics of a piezoelectric disk can be combined based on Eqs. (21) and (23). It can be seen that there are four equations and eight unknowns $[F_1, F_2, F_3, V, v_1, v_2, v_3, I]^T$ to be determined; therefore, four boundary conditions are needed to solve this vibration problem.

Taking piezoelectric disk shown in Fig. 1 for instance, one flat surface is attached to an aluminum plate with epoxy at the fixed end (see experimental set-up in Section 3) and the rest surfaces are surrounded by air. Then, the boundary conditions for stress-balance on each surface are

$$\begin{aligned} \frac{F_1}{A_1} - z_{air}v_1 &= 0, \\ \frac{F_2}{A_2} - z_{epo}v_2 &= 0, \\ \frac{F_3}{A_3} + z_{air}v_3 &= 0, \end{aligned} \tag{24}$$

where z_{air} and z_{epo} are the specific acoustic impedances of air and epoxy, respectively. Therefore, the overall equation set can be expressed in a matrix form as shown in Eq. (25). It is noted that, by setting an angular frequency ω in Eq. (25), the corresponding displacement amplitude at the free end (i.e., at $z = b$) can be obtained through time integral of v_3.

$$\begin{bmatrix} 0 \\ 0 \\ 0 \\ 0 \\ 0 \\ 0 \\ 0 \\ MV \end{bmatrix} = \begin{bmatrix} -1 & 0 & 0 & 0 & \frac{z_1(2\pi ab)}{j}\left[\frac{k_1 a J_0(k_1 a)-J_1(k_1 a)}{k_1 a J_1(k_1 a)} + \frac{c_{12}^D}{c_{11}^D k_1 a}\right] & \frac{2\pi a c_{13}^D}{j\omega} & \frac{2\pi a c_{13}^D}{j\omega} & \frac{-2bh_{31}M}{j\omega a} \\ 0 & -1 & 0 & 0 & \frac{2\pi a c_{13}^D}{j\omega} & \frac{z_3(\pi a^2)}{j\tan(k_3 b)} & \frac{z_3(\pi a^2)}{j\sin(k_3 b)} & \frac{-h_{33}M}{j\omega} \\ 0 & 0 & -1 & 0 & \frac{2\pi a c_{13}^D}{j\omega} & \frac{z_3(\pi a^2)}{j\sin(k_3 b)} & \frac{z_3(\pi a^2)}{j\tan(k_3 b)} & \frac{-h_{33}M}{j\omega} \\ 0 & 0 & 0 & -M & \frac{-2bh_{31}}{j\omega a} & \frac{-h_{33}}{j\omega} & \frac{-h_{33}}{j\omega} & \frac{M}{j\omega C_0} \\ \frac{1}{2\pi ab} & 0 & 0 & 0 & -z_{air} & 0 & 0 & 0 \\ 0 & \frac{1}{\pi a^2} & 0 & 0 & 0 & -z_{epo} & 0 & 0 \\ 0 & 0 & \frac{1}{\pi a^2} & 0 & 0 & 0 & z_{air} & 0 \\ 0 & 0 & 0 & M & 0 & 0 & 0 & 0 \end{bmatrix} \begin{bmatrix} F_1 \\ F_2 \\ F_3 \\ V \\ v_1 \\ v_2 \\ v_3 \\ I \end{bmatrix} \tag{25}$$

Remark 2 The expression shown in Eqs. (1)-(4) are so-called (S,D)-type expression. Since piezoelectric constants are usually provided in (T, E)-type (i.e., in terms of s_{IJ}^E, d_{iJ}, and ε_{ij}^T), the transformation are used as follows

$$\beta_{ij}^S = \left\{ \varepsilon_{ij}^T - d_{iJ}\left[d_{jJ}\left(s_{JJ}^E \right)^{-1} \right]' \right\}^{-1},$$

$$c_{IJ}^D = \left[s_{IJ}^E - d'_{iI}\left(\varepsilon_{ij}^T \right)^{-1} d_{iJ} \right]^{-1},$$

$$h_{iJ} = \left(\varepsilon_{ij}^T \right)^{-1} d_{jI} c_{IJ}^D,$$

where the symbol prime denotes the transpose of a matrix, and I, J = 1, 2, ..., 6; i, j = 1, 2, 3.

2.2 Sound field resulted from the vibration of a riezoelectric disk

The vibration of a piezoelectric disk is utilized in acoustic applications as it causes sound field into medium. Moreover, it can be envisioned that infinite sound point sources spread on the vibrating surface of a piezoelectric disk (Cheeke 2002), and emit spherical waves away. With Huygens-Fresnel principle, the amplitude and the phase could be seen as the interference from each sound point source (Dehn 1960) shown in Fig. 2 and summed according to the principle of superposition.

In Fig. 3, each infinitesimal area dA on the emitter (i.e., the piezoelectric disk; which vibrates with $u_z = v_3 e^{j(\omega t-\psi)}$ at the free end) produces a differential pressure dp at a point on the sensor surface in distance r', and this pressure dp can be expressed as (Cheeke 2002, Imamura 1991)

$$dp = \frac{j\rho_{air} c_{air} k_{air}}{2\pi r'} (v_3 dA)\, e^{j(\omega t-\psi-k_{air} r')}$$

where, c_{air} is the sound velocity in air, and $k_{air} = \dfrac{\omega}{c_{air}}$ is the wave number. From elementary geometry, the distance r' can be derived as

$$r' = \sqrt{\sigma_e^2 + \eta^2 - 2\eta\sigma_e \sin\phi \cos\theta_e}.$$

Then the incident pressure p_{in} on a point located at σ_s from the center of the sensor is the integral of dp over the surface of the piezoelectric disk, i.e.

$$p_{in}(\sigma_s) = \frac{j\rho_{air}c_{air}k_{air}v_3}{2\pi}\int_0^{2\pi}\int_0^{a_e}\frac{e^{j\left(\omega t-\psi-k_{air}r'\right)}}{r'}\sigma_e d\sigma_e d\theta_e \tag{26}$$

It can be seen that the incident pressure derived in Eq. (26) is a complex number which indicates phase shift from the emitter.

In practical pressure measurements, where the emitter and pressure sensor are usually set concentrically in a finite distance, reflected waves are continuously bounced back-and-forth, and the overall reflected waves make the measured pressure value higher than those measured in non-reflection cases. To depict the continuous bouncing effect, Huygens-Fresnel principle can be utilized during every wave reflection. In other words, for every reflection, the reflected wave will be considered as a new pressure source and it will generate pressure on the surface in front of it.

In order to describe the intensity of reflected waves in terms of incident waves, the reflection coefficient R_{re} from Ref. (Auld 1973) is utilized in this research

$$\frac{p_{re}}{p_{in}} = R_{re} = \frac{z_{re}-z_{in}}{z_{re}+z_{in}}, \tag{27}$$

where z_{in} is the specific acoustic impedance of medium that contains the incident and reflected waves, and z_{re} is the specific acoustic impedance of medium that contains the refracted wave (see Fig. 4).

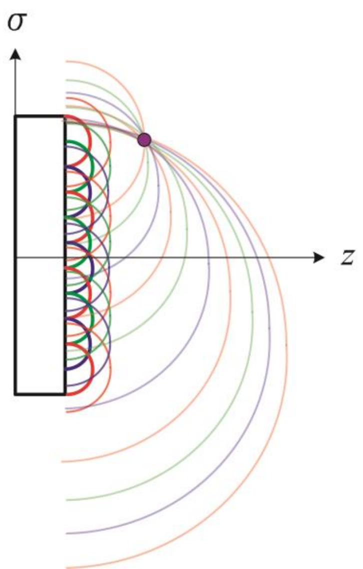

Fig. 2 Schematic diagram to show the interference of each spherical wave from a piezoelectric disk

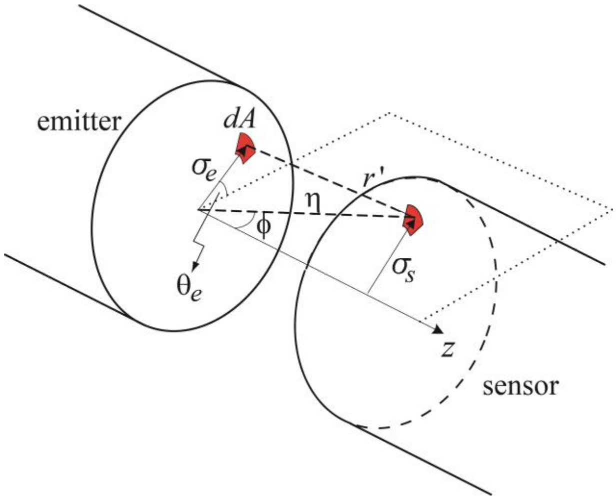

Fig. 3 Geometric relation between the emitter (piezoelectric disk) and the pressure sensor for sound field analysis

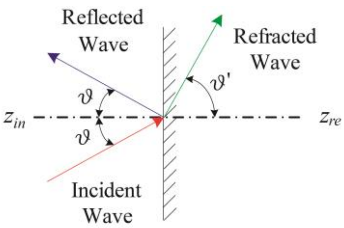

Fig. 4 Sound reflection and refraction at the boundary. Where z_{in} and z_{re} are the specific acoustic impedances; ϑ and ϑ' are the incident angle and the refraction angle, respectively

Thus, Eq. (26) can be modified to describe the pressure on the emitter and the sensor for every reflection as

$$\begin{aligned} p_{e,n}(\sigma_e) &= \frac{jk_{air}}{2\pi}\int_0^{2\pi}\int_0^{a_s} p_{s,n-1}(\sigma_s)R_{re,s}\frac{e^{j(\omega t-\psi-k\,r')}}{r'}\sigma_s d\sigma_s d\theta_s \\ p_{s,n}(\sigma_e) &= \frac{jk_{air}}{2\pi}\int_0^{2\pi}\int_0^{a_e} p_{e,n}(\sigma_e)R_{re,e}\frac{e^{j(\omega t-\psi-k\,r')}}{r'}\sigma_e d\sigma_e d\theta_e \end{aligned} \tag{28}$$

where n = 1, 2, 3 ⋯ , denotes the n^{th} reflection, $R_{re,e}$ and $R_{re,s}$ are the reflection coefficients of the emitter and the sensor, respectively. Moreover, the averaged amplitude of the overall pressure on the pressure sensor, $\overline{p}_{s,tot}$, can be predicted as,

$$\overline{p}_{s,tot} = \frac{1}{a_s}\int_0^{a_s}\left|\sum_{n=1}^{\infty} p_{s,n}(\sigma_s)\right| d\sigma_s, \tag{29}$$

which will be compared with the *experimental* result then.

Remark 3 $p_{s,0}(\sigma_s)$ in Eqs. (28) and (29) is the first incident pressure on the sensor, i.e., the pressure expressed in Eq. (26).

3. Experimental results and discussions

3.1 The resonant frequency of the piezoelectric disk

As shown in Fig. 5, one surface of the piezoelectric disk (PZT8, the properties are shown in Appendix) was fixed to an aluminum plate with epoxy and the rest surfaces were surrounded by air. In order to measure the displacement of the piezoelectric disk at the free end, a home-made position measuring device was utilized which consisted of a laser source, a photodiode, and an analog circuit. In particular, the laser source was placed in front of the piezoelectric disk with a large incident angle to magnify the displacement as shown in Fig. 6.

During the experiment, an AC voltage (100 Vpp) from the power amplifier (Model A-303 from A.A. LAB SYSTEMS LTD) was applied to the piezoelectric disk. Then, the vibration of the piezoelectric disk made the reflected light move back-and-forth on the bi-cell photodiode, and this signal was transformed by an analog circuit to the displacement. By varying the frequency of AC input, displacements of the piezoelectric disk at the free end could be obtained and plotted in Fig. 7.

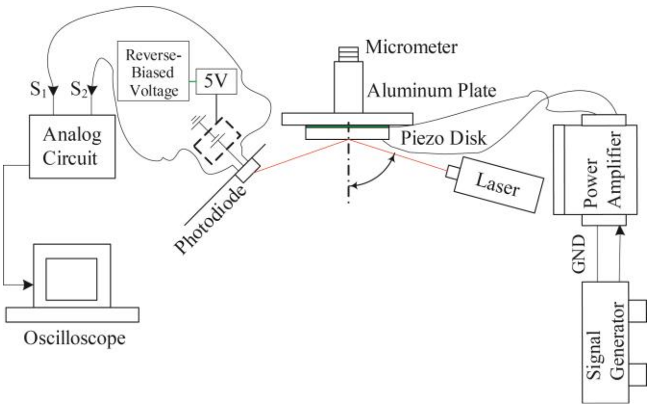

Fig. 5 Schematic diagram of the experimental set-up for measuring the displacement of the piezoelectric disk at the free end

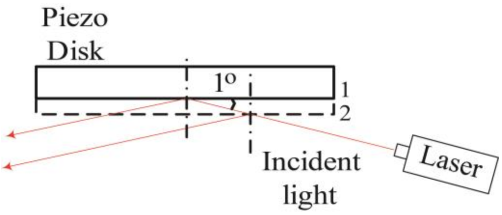

Fig. 6 Schematic diagram of optical magnification: position 1 and 2 indicate the deformation of piezoelectric disk in the thickness direction at different time instance

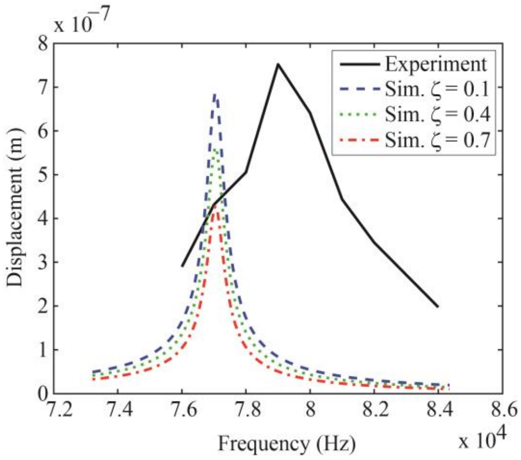

Fig. 7 Comparison of displacement of the piezoelectric disk at the free end for experimental result and theoretical analysis under different damping ratios ζ. The resonant frequency is around 77.03 *kHz* in theoretical analysis and 79.00 *kHz* in experiment. (note: the acoustic viscosities η corresponding to ζ=[0.1, 0.4, 0.7] are 44453($N{\cdot}s/m^2$), 177810($N{\cdot}s/m^2$), and 311170($N{\cdot}s/m^2$), respectively)

After inspecting the experimental results and comparing them with our theoretical analysis, some issues are worthy to be explored and elaborated as follows.

Proposed Vibration Model with Consideration of Gluing Material Can Predict the Resonant Frequency Precisely It can be seen in Fig. 7 that the predicted resonant frequency complies with the experimental result well and the discrepancy is less than 2.5%. In addition, the resonant frequency derived from different methods were compared in Table 1. It can be seen that the resonant frequency predicted in proposed vibration model was closest to that in experiment. Moreover, without considering the epoxy (which was used to glue the piezoeletric disk on the fixed end), the finite element method will give worse prediction.

The Acoustic Viscosity Affects the Amplitude of Displacement and Can be Determined via Experiment The amplitude of displacement will vary depending on different damping ratio ζ (see Fig. 7) and the damping ratio is a function of the acoustic viscosity η (see Eq. (11)), therefore, the acoustic viscosity of a material can be determined when the predicted peak displacement matches the experimental one.

Uncertainty of Material Properties Cause Significant Shift in the Predicted Displacement By utilizing sensitivity analysis, the effects of material properties on the predicted results are realized. In particular, three properties that affect the predicted results most are shown in Tables 2 and 3. It can be seen that ±20% uncertainty of s_{12}^E will cause shift of the resonant frequency and peak displacement less than ±5%. In contrast, ±20% uncertainty of s_{13}^E (or s_{23}^E) will cause tinny shift on the resonant frequency but above ±30% shift of the peak displacement. Therefore, since it is inevitable to have more or less errors between the real material properties and the nominal values, the displacement is more difficult to be predicted as precise as the resonant frequency.

3.2 Measuring the pressure resulted from the vibration of a piezoelectric disk

Fig. 8 shows the schematic diagram for pressure measurement. It can be seen that, cooperated with the position measuring device, a pressure sensor (Model ITC-9101 from International Transducer Corporation) was set in front of the piezoelectric disk on a movable stage such that the measuring position could be adjusted. It is noted that, the measured pressure is the result of infinite-times sound wave reflection between the piezoelectic disk and the pressure sensor. Therefore, it should be equal to Eq. (29).

Table 1 Comparison of the resonant frequency derived from different methods

Method	Resonant frequency (*kHz*)
Experiment	79.00
Coupled vibration Model	77.03
Finite element method with epoxy at the fixed end[†*]	82.40
Finite element method without epoxy at the fixed end[*]	102.90

[†] 1mm epoxy [*]Simulated with ANSYS (ANSYS, Inc.)

Table 2 The effect of compliance constant (s_{12}^E) uncertainty on the resonant freq. and displacement of our piezo-disk

s_{12}^E uncertainty (%)	Shift of resonant freq. (%)	Shift of peak displacement at resonant freq. (%)
-20	-4.03	0.11
-15	-3.00	0.57
-10	-2.07	0.80
-5	-1.03	0.65
0	0	0
5	1.14	-0.11
10	2.27	-0.45
15	3.41	-1.02
20	4.65	-1.18

[†] All simulation results are conducted by setting the acoustic viscosity η=44453 ($N{\cdot}s/m^2$) and the datum is the case that ζ=0.1 shown in Fig. 7 whose resonant frequency and resonant peak are 77.03 (*KHz*) and 6.87×10^{-7} (*m*), respectively

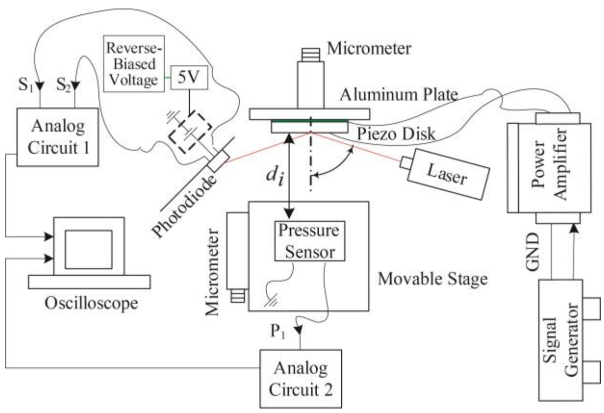

Fig. 8 Schematic diagram for measuring the pressure resulted from the vibration of a piezoelectric disk

Table 3 The effect of compliance constant ($s_{13}^E = s_{23}^E$) uncertainty on the resonant freq. and displacement of our piezo-disk

s_{13}^E *or* s_{23}^E uncertainty (%)	Shift of resonant freq. (%)	Shift of peak displacement at resonant freq. (%)
-20	-0.31	33.71
-15	-0.31	22.39
-10	-0.21	16.01
-5	-0.10	7.93
0	0	0
5	0.21	-6.90
10	0.41	-13.62
15	0.62	-20.06
20	0.93	-25.89

† All simulation results are conducted by setting the acoustic viscosity η=44453 ($N{\cdot}s/m^2$) and the datum is the case that ζ=0.1 shown in Fig. 7 whose resonant frequency and resonant peak are 77.03 (*KHz*) and 6.87×10^{-7} (*m*), respectively

Remark 4 Experiments were conducted by setting the pressure sensor at wave crests where the signals were more significant. Since where the wave crest appears is a function of frequency, the distance from the piezoelectric disk to wave crests under different frequencies is listed in Table 4 for reference).

In order to verify the concept for predicting the sound field shown in Sec. 2.2, the procedures are elaborated as follows. First, the initial vibration velocity (the time-derivative of the measured displacement in the first period, *i.e.*, no reflection happens) of the piezoelectric disk at the free end was plugged into Eq. (26) to derive the first incident pressure on the pressure sensor, $p_{s,0}(\sigma_s)$. Second, for deriving the reflected wave, the specific acoustic impedance is needed to calculate the reflection coefficient (see Eq. (27)). Since the medium between the pressure sensor and the piezoelectric disk is air, the reflection coefficients for pressure sensor and piezoelectric disk are

$$R_{re,s} = \frac{z_s - z_{air}}{z_s + z_{air}},$$

$$R_{re,e} = \frac{z_e - z_{air}}{z_e + z_{air}},$$

where z_{air} is the specific acoustic impedance of air, z_s is the specific acoustic impedance of the pressure sensor, and z_e is the specific acoustic impedance of the piezoelectric disk. Therefore, once all the acoustic impedances are known, pressures resulted from reflected waves each time can be calculated by Eq. (28). Based on the assumption of plane wave, z_{air} was calculated by multiplying air density with wave speed in the air at 25^oC, and z_e was set to be z_3 in Eq. (21) as

$$z_3 \equiv \rho_{pzt} c_3 = \rho_{pzt} \sqrt{\frac{c_{33}^D}{\rho_{pzt}}}.$$

However, the specification of z_s wasn't provided by the manufacturer and this led to a parameter search for the reflection coefficient $R_{re,s}$. An example can be seen in Fig. 9(a) that, reflection coefficient was searched at the second wave crest from the piezoelectric disk. Since there is an asymptotic pressure value that can match the measured pressure after infinite reflection times, the reflection coefficient $R_{re,s}$ is interpolated from two asymptotic pressure values that bound the measured pressure. At last, the reflection coefficient $R_{re,s}$ was used to predict the pressure at other position and compared to the experimental result as shown in Fig. 9(b) (a verification at the third wave crest).

It is noted that, for different vibration frequencies, the reflection coefficients $R_{re,s}$ are different and should be found separately with the approach shown above. Besides, in order to compare and quantify the discrepancy between the predicted pressure and the measured pressure (see Fig. 10 and Table 5), the error $Err_{p,i}$ was defined as

$$Err_{p,i} \equiv \frac{\left|p_{pre} - p_{mea}\right|}{p_{mea}} \times 100\%, \tag{30}$$

Table 4 Distance from the piezoelectric disk to wave crests where the pressure sensor was located

Frequency *(kHz)*	First wave crest position d_1 *(mm)*	Second wave crest position d_2 *(mm)*	Third wave crest position d_3 *(mm)*
78	2.51	4.76	7.02
79	2.47	4.69	6.95
80	2.44	4.61	6.85
81	2.41	4.55	6.75
82	2.36	4.48	6.65
83	2.36	4.42	6.55
84	2.34	4.38	6.48

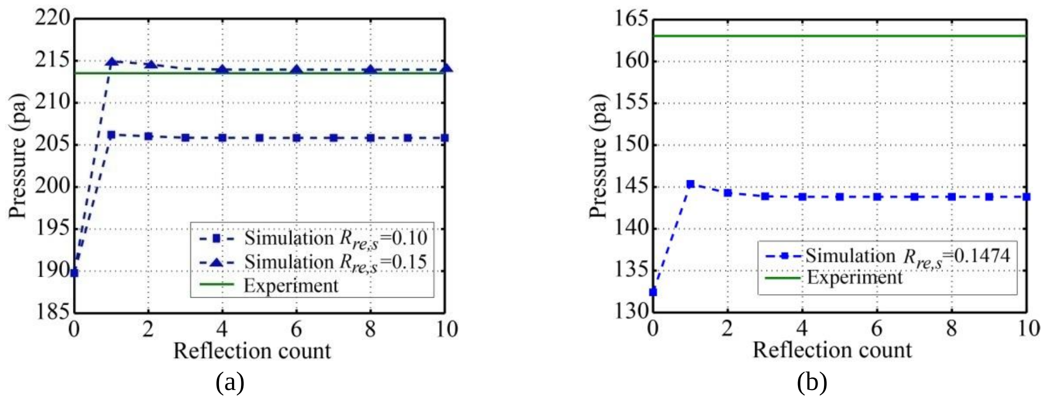

Fig. 9 An example of how to find the reflection coefficient of the pressure sensor when the piezoelectric disk vibrates at 80 *KHz*. (a) Reflection coefficient search at the second wave crest to the piezoelectric disk. (b) Pressure prediction at the third wave crest to the piezoelectric disk with interpolated reflection coefficient derived from (a)

Table 5 The interpolated reflection coefficient and the pressure error at the third wave crest

Frequency (*kHz*)	$R_{re,s}$	$Err_{p,3}$ (%)
78	0.8996	84.67
79	0.9644	26.97
80	0.1474	11.74
81	0.0440	15.08

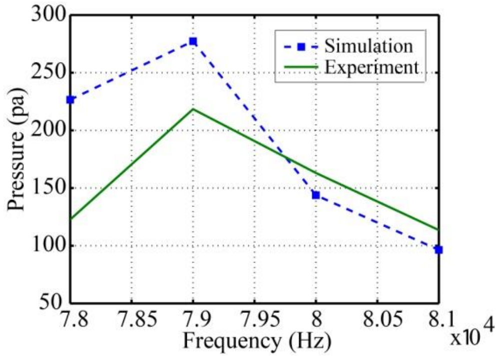

Fig. 10 Pressure at the third wave crest to the piezoelectric disk

Table 6 The interpolated reflection coefficient and the pressure error at the first wave crest

Frequency (*kHz*)	$R_{re,s}$	$Err_{p,1}$ (%)
78	0.8996	N/A†
79	0.9644	N/A†
80	0.1474	43.57
81	0.0440	33.17

†Simulation result diverged

where p_{pre} is the predicted pressure, p_{mea} is the measured pressure, and i specifies the position of i^{th} wave crest. It can be seen that the best prediction happened at 80 *KHz* with 11.74% error. However, at 78 *KHz*, the predicted pressure achieved 84.67% error.

The Assumption of Plane Wave Has Limitation on Predicting the Pressure The discrepancy between the predicted pressure and the measured results was illustrated with the specific acoustic impedance of air. It is noted that, the specific acoustic impedance of air, z_{air}, in spherical coordinate can be expressed from Ref. (Cheeke 2002) as

$$z_{air} = \rho_{air} c_{air} \frac{k_{air}^2 r^2}{1 + k_{air}^2 r^2} + j\rho_{air} c_{air} \frac{k_{air} r}{1 + k_{air}^2 r^2}, \tag{31}$$

where ρ_{air} is the air density, c_{air} is the wave velocity, k_{air} is the wave number, and r is the coordinate variable (or the propagation distance). As long as $k_{air}r$ is large enough, z_{air} will approach a real number like a plane wave; otherwise z_{air} should be a complex number. Taking the 80 *KHz* case for example, when measuring pressure at the third wave crest, the ratio of imaginary part to real part based on Eq. (31) is $\simeq$

$$\frac{1}{k_{air} r} = \frac{1}{k_{air} d_3} \simeq 0.101$$

Since the real part is about one-order larger than the imaginary part, assuming z_{air} to be a real number may deviate from the real situation, but won't be too bad. However, error may increase when $k_{air}r$ becomes smaller by either shortening the measuring distance or decreasing the vibration frequency to make wave number k_{air} smaller. Considering again the 80 *kHz* case, if the measuring position is moved to the first wave crest, the ratio of imaginary part to real part will increase to

$$\frac{1}{k_{air} r} = \frac{1}{k_{air} d_1} \simeq 0.28$$

which implies that plane wave is not a good assumption. Errors when predicting pressure at the first wave crest were listed in Table 6 to support this argument.

4. Conclusions

In this article, a coupled vibration model including energy dissipation was utilized, and a new problem solving procedure was proposed to predict the vibration behavior of a piezoelectric disk in the thickness direction. On the other hand, with an obstacle in a finite distance, the sound field resulted from the vibration of a piezoelectric disk was evaluated by Huygens-Fresnel principle involving an idea of continuous reflection. Results of the tested piezoelectric disk show that, discrepancies between the simulation and experiment are 2.5% for resonant frequency and 12% for resulted sound field. Besides comparing our simulation with experimental results, systematic analysis on where the discrepancy come from including uncertainty of material properties and modeling assumption were elaborated. In the future, the measuring system will be improved and a series of piezo-disks will be investigated to verify the feasibility of the proposed model further. We firmly believe that will get more accurate prediction and contribute to systematic design for piezoelectric-disk-based transducers.

Acknowledgments

Support from New-Faculty-Program of National Cheng-Kung University, Republic of China, is gratefully acknowledged.

References

Auld, B.A. (1973), *Acoustic Fields and Waves in Solids*, Wiley, New York, NY, USA.
Cheeke, J.D.N. (2002), *Fundamentals and Applications of Ultrasonic Waves*, CRC Press, Boca Raton, USA, chapter 6.
Dehn, J.T. (1960), "Interference patterns in the near field of a circular piston", *J. Acoust. Soc. Am.*, **32**(12), 1692–1696.
Ding, D., Zhang, Y. and Liu, J. (2003), "Some extensions of the gaussian beam expansion: Radiation fields

of the rectangular and the elliptical transducer", *J. Acoust. Soc. Am.*, **6**(113), 3043-3048.
Griffice, C.P. and Seydel, J.A. (1981), "Spherical wave decomposition approach to ultrasonic field calculations", *J. Nondestruct. Eval.*, **2** (3-4), 241-247.
Dugnani, R. (2009), "Dynamic behavior of structure-mounted disk-shape piezoelectric sensors including the adhesive layer", *J. Intell. Mat. Syst. Str.*, **20** (13), 1553-1564.
Guo, N., Cawley, P. and Hitchings, D. (1992), "The finite element analysis of the vibration characteristics of piezoelectric discs", *J. Sound Vib.*, **159**, 115-138.
Gutierrez, M.I., Calas, H., Ramos, A., Vera, A. and Leija, L. (2012), "Acoustic field modeling for physiotherapy ultrasound applicators by using approximated functions of measured non-uniform radiation distributions", *Ultrasonics*, **52** (6), 767-777.
Huang, C.H., Lin, Y.C. and Ma, C.C. (2004), "Theoretical analysis and experimental measurement for resonant vibration of piezoceramic circular plates", *IEEE T. Ultrason. Ferr.*, **51**(1), 12-24.
IEEE Standard (1987), *IEEE Standard on Piezoelectricity*, IEEE Standards Board, American National Standards Institute.
Ikeda, T. (1990), *Fundamentals of Piezoelectricity*, Oxford University Press, Oxford, UK, chapter 2.
Imamura, T. (1991), "Particle velocity and acoustic impedance density of the ultrasonic field by the circular flat transducers", *J. Acoust. Soc. Jpn*, **12**(3), 115-122.
Iula, A., Lamberti, N. and Pappalardo, M. (1998), "An approximated 3-d model of cylinder-shaped piezoceramic elements for transducer design", *IEEE IEEE T. Ultrason. Ferr.*, **45** (4), 1056-1064.
Kocbach, J. (2000), *Finite element modeling of ultrasonic piezoelectric transducers*, Ph.D. Dissertation, University of Bergen, Bergen, Norway.
Kung, Y.S. and Fung, R.F. (2002), "Precision control of a piezoceramic actuator using neural networks", *Proceedings of the 2002 28th Annual Conference of the IEEE Industrial Electronics Society*, Sevilla, Spain, November.
Kunkel, H.A., Locke, S. and Pikeroen, B. (1990), "Finite-element analysis of vibrational modes in piezoelectric ceramic disks", *IEEE T. Ultrason. Ferr.*, **37** (4), 316–328.
Lee, J.R., Park, C.Y. and Kong, C.W. (2013), "Simultaneous active strain and ultrasonic measurement using fiber acoustic wave piezoelectric transducers", *Smart Struct. Syst.*, **11** (2), 185-197.
Lee, P.C.Y., Liu, N. and Ballato, A. (2004), "Thickness vibrations of a piezoelectric plate with dissipation", *IEEE T. Ultrason. Ferr.*, **51**(1), 52-62.
Lin, S., Fu, Z., Zhang, X., Wang, Y. and Hu, J. (2013), "Radially sandwiched cylindrical piezoelectric transducer", *Smart Mater. Struct.*, **22** (1), 1-10.
Lin, S.Y. (1998), "Coupled vibration analysis of piezoelectric ceramic disk resonators", *J. Sound Vib.*, **218**(2), 205-217.
Liu, J., Ono, K., Xu, J., Li, J. and Furukawa, M. (2012), "Thermal actuator for accurate positioning read/write element in hard disk drive", *Microsyst. Technol.*, **18**(9-10), 1583-1589.
Martins, M., Correia, V., Cabral, J.M., Lanceros-Mendez, S. and Rocha, J.G. (2012), "Optimization of piezoelectric ultrasound emitter transducers for underwater communications", *Sensor. Actuat. A – Phys.*, **184**, 141-148.
Nowotny, H. and Benes, E. (1987), "General one-dimensional treatment of the layered piezoelectric resonator with two electrodes", *J. Acoust. Soc. Am.*, **2**(82), 513-521.
Tiersten, H.F. (1963), "Thickness vibrations of piezoelectric plates", *J. Acoust. Soc. Am.*, **35** (1), 53-58.
Wang, B.T. (1996), "Optimal placement of microphones and piezoelectric transducer actuators for far-field sound radiation control", *J. Acoust. Soc. Am.*, **5**(99), 2975-2984.
Zenz, G., Berger, W., Gerstmayr, J., Nader, M. and Krommer, M. (2013), "Design of piezoelectric transducer arrays for passive and active modal control of thin plates", *Smart Struct. Syst.*, **12** (5), 547-577.

CC

Appendix

The piezoelectric constants used in this research in Voigt's notation are as follows,

$$s^E = \begin{bmatrix} 12.1 & -3.7 & -4.8 & 0 & 0 & 0 \\ -3.7 & 12.1 & -4.8 & 0 & 0 & 0 \\ -4.8 & -4.8 & 13.5 & 0 & 0 & 0 \\ 0 & 0 & 0 & 31.9 & 0 & 0 \\ 0 & 0 & 0 & 0 & 31.9 & 0 \\ 0 & 0 & 0 & 0 & 0 & 31.6 \end{bmatrix} * 10^{-12} \left(\frac{m^2}{N} \right),$$

$$d = \begin{bmatrix} 0 & 0 & 0 & 0 & 330 & 0 \\ 0 & 0 & 0 & 330 & 0 & 0 \\ -110 & -110 & 250 & 0 & 0 & 0 \end{bmatrix} * 10^{-12} \left(\frac{m}{V} \right),$$

$$\varepsilon^T = \begin{bmatrix} 1290 & 0 & 0 \\ 0 & 1290 & 0 \\ 0 & 0 & 1030 \end{bmatrix} * 8.854 * 10^{-12} \left(\frac{F}{m} \right).$$

List of Symbols

a	radius [*m*]
b	thickness [*m*]
c	wave propagation velocity [*m/s*]
c_{ij}^{D}	elastic constant under constant electric displacement [N/m^2]
d_i	distance from the emitter to the i^{th} wave crest [*m*]
d_{iJ}	piezoelectric constant in Voigt's notation [*m/V*]
h_{iJ}	piezoelectric constant [*N/C*]
k	wave number [*rad/m*]
p	pressure [N/m^2]
s_{IJ}^{E}	compliance constant under constant electric field in Voigt's notation [m^2/N]
u_i	displacement toward *i*-direction [*m*]
v_i	vibration velocity on surface-*i* [*m/s*]
z	specific acoustic impedance [$Kg/(m^2 \cdot s)$]
D_i	electric displacement toward *i*-direction [C/m^2]
E_i	electric field toward *i*-direction [*V/m*]
F_i	force on surface-*i* [*N*]
I	amplitude of induced alternating current [*A*]
R_{re}	reflection coefficient [-]
S_{ij}	strain that points to *j*-direction resulted from the force applied on normal-plane-*i* [-]
T_{ij}	stress that points to *j*-direction resulted from the force applied on normal-plane-*i* [N/m^2]
U_i	displacement amplitude toward *i*-direction [*m*]
V	voltage [*V*]
β_{ij}^{S}	dielectric impermeability at constant strain [*m/F*]
ε_{ij}^{T}	permittivity constant under constant stress [*F/m*]
η	acoustic viscosity [$(N \cdot s)/m^2$]
ρ	density of a material [Kg/m^3]
ψ	phase delay [*rad*]
ω	angular frequency [*rad/s*]

Subscripts

air	air related
e	emitter related
i, j	index of tensor form (i, j=1~3)
in	incident component
pzt	pzt related
re	reflected component
r, θ, z, ϕ	in a given direction
s	sensor related
tot	total quantity
I, J	index of tensor form (I, J=1~6)